An analytical model of nonproportional scintillator light yield in terms of recombination rates

G. Bizarri[a], W.W. Moses[a], J. Singh[b] , A.N. Vasil'ev[c], and R.T. Williams[d]

[a] *Lawrence Berkeley Lab., Berkeley, CA 94720-8119, USA*
[b] *School of Engineering and IT, Charles Darwin University, Darwin, NT 0909, Australia*
[c] *Institute of Nuclear Physics, Moscow State University, Moscow 119991, Russia*
[d] *Department of Physics, Wake Forest University, Winston-Salem, NC 27109, USA*

Abstract

Analytical expressions for the local light yield as a function of the local deposited energy (-*dE/dx*) and total scintillation yield integrated over the track of an electron of initial energy *E* are derived from radiative and/or nonradiative rates of first through third order in density of electronic excitations. The model is formulated in terms of rate constants, some of which can be determined independently from time-resolved spectroscopy and others estimated from measured light yield efficiency as a constraint assumed to apply in each kinetic order. The rates and parameters are used in the theory to calculate scintillation yield versus primary electron energy for comparison to published experimental results on four scintillators. Influence of the track radius on the yield is also discussed. Results are found to be qualitatively consistent with the observed scintillation light yield. The theory can be applied to any scintillator if the rates of the radiative and non-radiative processes are known.

1. Introduction

The light yield of scintillators has attracted research interest for decades [1] because of their applications in medical imaging [2], homeland security detectors [3], radiation detectors [4], etc. The scintillation yield (Y) is defined as the total energy of emitted photons (E_p) per unit energy (E) deposited by the incident particle or gamma-ray in a scintillator material, i.e. $Y = E_p/E$ [5]. The experimentally observed scintillation yield is found not to be a constant but to vary with E, a phenomenon known as non-proportionality [1] in the scintillator response . A constant light yield implies that the scintillator is "proportional" and that means the amount of scintillation light generated is proportional to the amount of energy deposited into the scintillator. Although scintillators have been known for many decades, it is not yet clearly understood what causes the non-proportionality. In fact, the issue has been addressed in so many ways that it has even created some confusion in the literature [1,5].

The emission of photons from a scintillator occurs because the incident radiation first creates a pair of a very high energy excited electron and hole, which then lose energy in a cascade that produces a track of generally high density excited electron-hole (e-h) pairs. Some of these excitations finally recombine radiatively and generate photons which can be detected and constitute the "scintillator response". If the excited e-h pairs recombine only radiatively without going through any other processes of losing their energy, then one can expect a "proportional" scintillator response. However, the creation of high density excitations in scintillators involves various other types of radiative and non-radiative processes among the excitations and the light yield becomes a complicated function of the rates of all these processes. As the rates of these processes may be expected to vary from one material to another, different materials may exhibit different forms of non-proportionality, as indeed it has been observed [6]. In order to understand the non-

proportionality in scintillators it is therefore important to study various processes of interaction occurring in a high excitation density situation in a scintillating crystal when it is subjected to a high energy incident radiation (particle) that can create high density excitations along its trajectory.

In insulators and semiconductors, an incident energy larger than the band gap energy (but smaller than the threshold of multiplication of electronic excitations) excites an e-h pair, which loses the excess energy above the band gap non-radiatively to lattice vibrations, usually in the pico-second or even shorter time range. In semiconductors some of these relaxed e-h pairs, but not all, may recombine radiatively by emitting a photon, whose energy is equal to the band gap energy. Some of the free e-h pairs may form excitons due to their Coulomb interaction and get bound in hydrogen-like energy states and the excess energy equal to the binding energy is again lost to the lattice non-radiatively. These excitons are called free excitons (FE) and can recombine radiatively by emitting a photon of energy less than the band gap energy, called FE photoluminescence (PL). Free exciton PL and direct radiative electron-hole recombination is usually observed in crystals with little to very small charge carrier-lattice interaction. Such crystals are usually known to be quite rigid in their structure. For scintillators, the crystals used are ionic and organic solids, which have strong charge carrier-lattice interaction and hence not as rigid. In such crystals, the excited e-h pairs can undergo further non-radiative relaxation due to the lattice interaction and form what are called self-trapped excitons (STE). STE can then recombine radiatively by emiting photons, called STE photoluminescence, which occurs at an energy less than FE PL. In some crystals, usually organics, both FE and STE have been observed to co-exist [7]. These three radiative processes and associated non-radiative processes are known to be linear and if these are the only processes that occur in a scintillator, which may be possible at a very low excitation density, then it may be expected to give a proportional response.

In this paper, a phenomenological approach is presented to study the scintillator response of a scintillator by including the rates of linear, binary and ternary (Auger) processes in the rate equations. It is considered that initially one creates a number of excitations, some of which form excitons before their radiative recombination and some remain e-h pairs. The exchange between e-h pairs and excitons is also possible and considered. First the general theory is developed and approximate expressions for the local light yield (Y_L) and total light yield (Y) are derived as functions of different rates of recombination. Then the results are applied to calculate the scintillator response, both local and total light yields in four scintillating crystals, NaI:Tl, BaF_2, Gd_2SiO_5:Ce (GSO) and $LaCl_3$:Ce. As these four scintillators have been widely studied experimentally and used as scintillators, results obtained here can easily be compared with experiments. Rates of recombination are extracted from experiments where possible, and in other cases by estimation as discussed. When it was necessary to estimate rates or other parameters, we tried to impose the estimated values as constants across all four materials, to avoid using estimated parameters as fitting variables. The dependence of the light yield on different recombination rates and track radius is investigated. A qualitative agreement is found with the experimental yields. The theory is general and if the rates are known the light yield can be calculated for any scintillator.

The paper is organized as follows: In section 2, the general theory is developed and approximate expressions for the local (Y_L) and total (Y) light yields are derived. In section 3, the theory is used to calculate the light yields in four scintillators, NaI:Tl, BaF_2, GSO and $LaCl_3$:CE, representing different importance of first and second order recombination processes. A description on how various rates are obtained is also presented in section 3. A discussion of the theory developed is presented in section 4, which contains two subsections 4.2 and 4.3 presenting discussions on the validity of track structure model (namely the radial and axial distribution of excitations within the track region) used for our analytical estimations.

2. Rate Equations

We include in the rate equations only excitons and pairs of electron and hole (e-h pairs) that are generated by an incident γ -quantum in a scintillating crystal. Aside from the exciton and carrier populations, plasmon excitation is considered at an earlier stage in the calculation of electronic excitation density involving the dielectric function (Section 4.3). Furthermore, phonons are generated in relaxation of energetic carriers and self-trapping of excitons. Here we consider the model of a cylindrical track of radius *r* with a stepwise dependence of exciton and carrier concentration in radial direction. Such a cylindrical track has also been recently applied by Jaffe [8]. The applicability of this model will be discussed in section 4. The dynamical changes in exciton and e-h pair densities at any point, *x*, along the track can be expressed by the following two rate equations:

$$-\frac{dn_{ex}(x)}{dt} = (R_{1x} + K_{1x})n_{ex}(x) + (R_{2x} + K_{2x})n_{ex}^2(x) - \gamma_{ex}n_{eh}(x) + \gamma_{xe}n_{ex}(x) + K_{3x}n_{ex}(x)^3 - f_x n(x)\delta(t), \quad (1)$$

$$-\frac{dn_{eh}(x)}{dt} = (R_{1eh} + K_{1eh})n_{eh}(x) + (R_{2eh} + K_{2eh})n_{eh}^2(x) - \gamma_{xe}n_{ex}(x) + \gamma_{ex}n_{eh}(x) + K_{3eh}n_{eh}^3(x) - (1 - f_x)n(x)\delta(t), \quad (2)$$

where $n_{ex}(x)$ is the excitonic concentration and $n_{eh}(x)$ is the concentration of excited e-h pairs not bound like excitons at any point *x* on the beam track. f_x is the fraction concentration of excitons , $(1 - f_x)$ is the fraction concentration of e-h pairs, and $n(x)\delta(t)$ represents the total number of excitations, $n(x) = n_{ex}(x) + n_{eh}(x)$, created by the incident energy at time $t = 0$ at any point *x* along the track. Accordingly, $n(x)$ (cm^{-3}) is defined as:

$$n(x) = \frac{\left(-\frac{\partial E}{\partial x}\right)}{\pi r^2 E_{eh}}, \qquad (3)$$

where E is the total initial energy incident at any point x, πr^2 is the average area of cross section of the track and E_{eh} is the average energy required to create an excitation in a scintillator, and here it is assumed to be three times the band gap energy (E_g) : $E_{eh} = 3E_g$ [8]. The validity of this approximation and the estimation of the track radius will also be discussed in section 4.

In Eqs. (1) and (2), R_{ix} and K_{ix} denote the rates of radiative and non-radiative (quenching) recombination of excitons, respectively, and i = 1, 2, denote through linear (1) and binary (2) processes. (R_{2x}, the rate of *radiative* exciton decay promoted by exciton-exciton interaction, is a known 2nd order luminescence channel in several semiconductors including ZnO, where it accounts for a distinct "p band" [9] of emission promoted by exciton-exciton scattering that leaves one exciton on the radiative polariton branch (hence promotion of rate) and the other exciton in an internal excited state (hence shifting of the p-band energy). However in Section 3.1 and Table 1, we shall declare $R_{2x} = 0$ for the four scintillators under present consideration, since there is no report of p-band emission for any of them.) R_{ieh} and K_{ieh} (i = 1, 2) are the corresponding rates of recombination for an e-h pair, and K_{3x} and K_{3eh} are rates of non-radiative Auger (ternary) recombination of excitons and an e-h pairs, respectively. It is assumed here that Auger processes do not contribute to any radiative recombination. γ_{ex} and γ_{xe} are rates of converting an eh pair into an exciton and vice versa, respectively. This is important to consider both the possibilities for applying the theory at higher temperatures. According to Eqs. (1) and (2), we can classify scintillators in three categories: (i) excitonic with $f(x) = 1$, (ii) non-excitonic with $f(x) = 0$, and (iii) mixed case $0 < f(x) < 1$.

It may also be important to note that the rate of any order in Eqs. (1) and (2) represents the sum of all the rates in that order. For example, R_{1x} represents the sum of the first order excitonic rates of radiative recombination of all possible channels, including recombination through doped impurities. $R_{1x} = R_{1x}^{STE} + R_{1x}^{ad}$, where R_{1x}^{STE} and R_{1x}^{ad} are rates of recombination of an intrinsic self-trapped excitons (STE) and through an activator impurity atom, respectively. Both processes contribute to the scintillation light yield.

2.1 Local Light Yield (Y_L)

If one integrates Eqs. (1) and (2) over time, one gets:

$$0 = (R_{1x} + K_{1x}) < n_{ex}(x) > +(R_{2x} + K_{2x}) < n_{ex}^2(x) > -\gamma_{ex} < n_{eh}(x) > +\gamma_{xe} < n_{ex}(x) > +K_{3x} < n^3{}_{ex}(x) > - f_x n(x)$$

,

(4)

$$0 = (R_{1eh} + K_{1eh}) < n_{eh}(x) > +(R_{2eh} + K_{2eh}) < n_{eh}^2(x) > -\gamma_{xe} < n_{ex}(x) > +\gamma_{ex} < n_{eh}(x) > +K_{3eh} < n_{eh}^3(x) > - (1 - f_x) n(x)$$

(5)

where $< n(x) >$ represents the integrated value of $n(x)$ over time, and

$\int_{0^-}^{\infty} \frac{dn(x)}{dt} dt = n(x)_{|\infty} - n(x)_{|0^-} = 0$ is used in arriving at Eqs. (4) and (5). It is obvious that Eqs. (4) and (5) have similar forms as Eqs. (1) and (2) in the steady-state but with unintegrated concentrations.

Adding Eqs. (4) and (5) we get:

$$(R_{1x} + K_{1x}) < n_{ex}(x) > +(R_{2x} + K_{2x}) < n_{ex}^2(x) > +(R_{1eh} + K_{1eh}) < n_{eh}(x) > +(R_{2eh} + K_{2eh}) < n_{eh}^2(x) > + K_{3eh} < n_{eh}^3 >= n(x)$$

(6)

Using Eq. (6), the local light yield (*YL*) at any point *x* along the track can be defined by:

$$Y_L = \frac{R_{1x} < n_{ex}(x) > + R_{2x} < n_{ex}^2(x) > + R_{1eh} < n_{eh}(x) > + R_{2eh} < n_{eh}^2(x) >}{n(x)}, \qquad (7)$$

where the numerator consists of only terms of the radiative processes in Eq. (6). Y_L in Eq. (7) is defined as the local light yield, which means the instantaneous yield at any point x along the track and it can be calculated provided all the rates and $< n_{ex}(x) >$, $< n_{ex}^2(x) >$, $< n_{ex}^3(x) >$, $< n_{eh}(x) >$, $< n_{eh}^2(x) >$ and $< n_{eh}^3(x) >$ are known. Latter ones can probably be determined in more than one way, but here we have estimated these using the linear order approximation. The details of the derivations are given in appendix A. According to Eq. (A.17), the local light yield is obtained as:

$$Y_L = \frac{a_1 + a_2 n(x)}{1 + a_3 n(x) + a_4 n(x)^2}, \qquad (8)$$

where the constants a_1, a_2, a_3, and a_4 are given in Eqs. (A.18) – (A.21).

In Eq. (3), using $E_{eh} = 3E_g$, we get the relation between $n(x)$ (cm^{-3}) and the deposited energy $-\frac{dE}{dx}$ at any point x along the track as:

$$n(x) = \frac{1}{3\pi r^2 E_g}(-\frac{dE}{dx}) \quad , \qquad (9)$$

Substituting Eq. (9) in Eq. (8) the local yield can be calculated as a function of $(-\frac{dE}{dx})$ (keV/cm) for any scintillating crystal. Such graphs of Y as a function of $(-\frac{dE}{dx})$ can be plotted and compared with previous results [6, 10].

2.2 Total ScintillationYield (*Y*)

However, recent experiments are carried out to measure the total scintillation light yield as a function of the total energy deposited by an incident γ -ray in a scintillator [11]. That means one

needs to find the total number of photons generated by the whole incident energy divided by the total number of excitations generated. This can be achieved by integrating the numerator and denominator of the local yield in Eq. (A16) over the whole track length and then one gets the total yield, Y as:

$$Y = \frac{(R_{1x}A + R_{1eh}B)n + (\frac{1}{2\tau_x}R_{2x}A^2 + \frac{1}{2\tau_{eh}}R_{2eh}B^2)\bar{n}^2}{[((R_{1x}+K_{1x})A + (R_{1eh}+K_{1eh})B)n + (\frac{1}{2\tau_x}(R_{2x}+K_{2x})A^2 + \frac{1}{2\tau_{eh}}(R_{2eh}+K_{2eh})B^2)\bar{n}^2 + \\ + (\frac{1}{3\tau_x^2}K_{3eh}A^3 + \frac{1}{3\tau_{eh}^2}K_{3eh}B^3)\bar{n}^3]} \tag{10}$$

Dividing the numerator and denominator of Eq. (10) by $((R_{1x}+K_{1x})A + (R_{1eh}+K_{1eh})B)n$, we can write Y as:

$$Y = \frac{a_1 + a_2(\bar{n}^2/n)}{1 + a_3(\bar{n}^2/n) + a_4(\bar{n}^3/n)}, \tag{11}$$

where $n = \frac{1}{L}\int_0^L n(x)dx$, $\bar{n}^2 = \frac{1}{L}\int_0^L n^2(x)dx$, $\bar{n}^3 = \frac{1}{L}\int_0^L n^3(x)dx$ and L denotes the total track length. It is to be noted that $\bar{n}^2$ and $\bar{n}^3$ are not the squared and cubed of n, respectively. However for evaluating these integrals we need to know ($-dE/dx$) in Eq. (9) as a function of the local energy incident at each point. There are many approaches for determining ($-dE/dx$), including the calculation of energy loss function $\mathrm{Im}\left(-\varepsilon^{-1}(\omega,q)\right)$ in a number of approximations (see, e.g., [12-16]). In order to obtain analytical formulas for calculating the total yield, in section 2.3 we have used an analytical form of ($-dE/dx$) derived from the Bethe-Bloch equation [17]. This form does not depend on the detailed description of energy loss function but on average ionization energy of the ions constituting the crystal and hence easy to use for analytical derivations. Later in Sec. 4.3 we

have discussed the more detailed evaluation of (*-dE/dx*) based on the numerical calculations of energy loss function.

2.3 Form of (*-dE/dx)*

Stopping power given by the modified (non-relativistic) Bethe equation [18] is:

$$-\frac{dE}{dx} = \frac{2\pi e^4 \kappa^2 \rho_e}{E} \ln\{(\frac{2.71}{2})^{1/2}[(E + 0.81I)/I]\}, \qquad (12)$$

where $\kappa = (4\pi\varepsilon_0)^{-1} = 8.9877 \times 10^9$, E is the total initial incident energy of gamma rays at any point *x* along its track, *I* is the average ionization energy and ρ_e is the electron density given by:

$$\rho_e = \frac{N_A Z \rho}{A}, \qquad (13)$$

where $N_A = 6.022 \times 10^{23}$ is the Avogadro number, *Z* and *A* are the atomic number and atomic weight number, respectively and ρ is the density of the material. A similar form of (*-dE/dx*) has recently been used by Jaffe [8]. Substituting Eq. (12) in Eq. (9) we get:

$$n(x) = \frac{2e^4 \kappa^2 \rho_e}{3r^2 E_g E} \ln\{1.164[E + 0.81I]/I\} \ . \qquad (14)$$

Using Eq. (9), the first integral of $n(x)$ can easily be evaluated as:

$$n = \frac{1}{3\pi r^2 E_g}[\frac{1}{L}\int_0^L (-\frac{dE}{dx})dx] = \frac{1}{3\pi r^2 E_g}[\frac{1}{L}\int_0^E (-\frac{dE}{dx})(\frac{dx}{dE})dE = \frac{1}{3\pi r^2 E_g}[\frac{E}{L}], \qquad (15)$$

where E is the total incident energy of the γ-ray. It is interesting to note that the total concentration n in Eq. (15) does not depend on the mathematical form of $(-\frac{dE}{dx})$ but higher powers of $n(x)$ do. Using Eqs. (9), (12) and (14), we can also integrate $n(x)^2$ and $n(x)^3$ over the track length as:

$$\overline{n}^2 = \frac{1}{L}\int_0^L n^2(x)dx] = \frac{1}{(3\pi r^2 E_g)^2}[\frac{1}{L}\int_0^E (-\frac{dE}{dx})^2(\frac{dx}{dE})dE = \frac{\pi e^4 \kappa^2 \rho_e}{(3\pi r^2 E_g)^2 L} A, \quad (16)$$

where

$$A = \{\ln[1.164(E + 0.81I)/I]\}^2 , \quad (17)$$

and

$$\overline{n}^3 = \frac{1}{L}\int_0^L n^3(x)dx] = \frac{1}{(3\pi r^2 E_g)^3}[\frac{1}{L}\int_0^E (-\frac{dE}{dx})^3(\frac{dx}{dE})dE = \frac{1.164(2\pi e^4 \kappa^2 n_e)^2}{L(3\pi r^2 E_g)^3 I A_t}[2A_t - (\ln(A_t))^2 - 2\ln(A_t) - 2] , \quad (18)$$

where

$$A_t = \{1.164(E + 0.81I)/I]\} . \quad (19)$$

Using Eqs (15), (16) and (18) we get:

$$(\overline{n}^2/n) = \frac{e^4 \kappa^2 \rho_e}{(3r^2 E_g)\ E} A, \quad (20)$$

$$(\overline{n}^3/n) = \frac{1.164}{A_t I E}\left(\frac{2e^4 \kappa^2 \rho_e}{3r^2 E_g}\right)^2 [2A_t - (\ln(A_t))^2 - 2\ln(A_t) - 2]. \quad (21)$$

Using Eqs. (20) and (21) in Eq. (11) the total yield Y can be obtained as a function of the total incident energy E .

2.4 Strictly excitonic excited state ($f_x = 1$)

Although the light yield for any value of the fraction excitonic concentration f_x can be calculated from Eqs. (8) and (11), two cases of $f_x = 0$ and 1 are special because then the two rate equations [Eqs. (1) and (2)] reduce into one equation. Considering only the non-zero rates in tables 1, the rate equation [Eq. (1)] for $f_x = 1$ reduces to:

$$-\frac{dn_{ex}(x)}{dt} = (R_{1x} + K_{1x})n_{ex}(x) + K_{2x}n_{ex}^2(x) + K_{3x}n_{ex}^3 - n(x)\delta(t) \quad . \tag{22}$$

Following the steps from Eqs. (4) to (7) and those in the appendix, the light yield in Eq. (8) reduces to Y_{exL} as:

$$Y_{exL} = \frac{a_1}{1 + a_3 n(x) + a_4 n(x)^2}, \tag{23}$$

where $a_1 = \frac{R_{1x}}{(R_{1x} + K_{1x})}$, $a_3 = \frac{K_{2x}}{2(R_{1x} + K_{1x})}$ and $a_4 = \frac{K_{3x}}{3(R_{1x} + K_{1x})}$.

It can be seen that the local light yield in Eq. (23) is a monotonically decreasing function of excitation density in this case. Such dependences are suggested by the BaF_2 and GSO data which are compared with the theory in Section 3.

2.5 Strictly electron and hole excited state ($f_x = 0$)

This case is the other extreme and here also the two rate equations reduce to one equation as:

$$-\frac{dn_{eh}(x)}{dt} = K_{1eh}n_{eh}(x) + R_{2eh}n_{eh}^2(x) + K_{3eh}n_{eh}^3(x) - n(x)\delta(t), \qquad (24)$$

where again only the non-zero rates in table 1 are considered. In this case the light yield in Eq. (8) becomes Y_{ehL} as:

$$Y_{ehL} = \frac{a_2 n(x)}{1 + a_3 n(x) + a_4 n(x)^2}, \qquad (25)$$

where

$$a_2 = a_3 = \frac{R_{2eh}}{2K_{1eh}}, \text{ and } a_4 = \frac{K_{3eh}}{3K_{1eh}}. \qquad (26)$$

Equation (25) produces scintillation light yield curves that rise and/or fall versus excitation density, depending on the relative values of a_2 and a_3, and a_4. The experimental scintillation yield curves for NaI:Tl and $LaCl_3$:Ce discussed in Section 3 exhibit this character in at least partial degree.

3. Extraction of rates from Experiments and Results

It is obvious that for calculating both local light yield (Y_L) [Eq. (8)] and total light yield (Y) [Eq. (11)] we need to know the rates of the various processes considered above in a scintillator. We have attempted to calculate the light yield for four scintillators: – NaI:Tl, BaF_2, GSO:Ce and $LaCl_3$:Ce using rates that are deduced from independent measurements where possible. In most cases where rates cannot be deduced independently, we have set them constant across all four materials, in order to avoid attributing differences between materials to arbitrary parameters. With such an approach, we do not obtain "good fits", but rather look for whether the main qualitative behaviours are

attributable to known rates and parameters. Although there are apparently a great many parameters in this model, from the discussion to follow, it turns out that only a few of the parameters are sensitive controllers of the shapes and the placement along the energy scale.

An important set of nonproportionality data spanning 10 scintillator materials has resulted from the measurement of scintillation yield excited by single Compton scattered electrons in the experiments of Mengesha et al. [11] shown in Fig. 1. Relative light output, normalized to the total light yield (Y) at the highest electron energy in each case, is plotted versus initial energy (E) of the primary Compton-scattered electron responsible for the light pulse. The following broad characterizations are suggested by inspection of the data:

- There are two basic varieties of the shapes of the plots. The simplest basic shape shared by some scintillators is a curve that is horizontal at the highest primary electron energies, and then rolls off smoothly as the primary electron energy decreases (See Fig. 1 (a)). These include GSO:Ce and BaF_2, and seem to match the monotonically decreasing Y_L versus n(x) in Eq. (23).
- Furthermore, the curves roll off in parallel fashion, suggesting commonality of the physical process responsible for the roll-off. The clustering of many of the curves almost on top of each other suggests that the physical parameters controlling the roll-off have about the same value in all of the clustered materials. YAP appears exceptional, although its data exist only for the higher primary electron energies and so we don't yet know if or when it turns over.
- The second basic shape is exhibited by the activated alkali halides, specifically NaI:Tl, CsI:Tl, and CsI:Na (see Fig. 1(b)). In these cases, the light yield rises as primary electron energy decreases from the highest value, reaches a peak, and then rolls off with further decrease of the primary electron energy. Within the known range of materials for which *Y*

versus E measurements have been made, this shape has been found *only* in activated halide scintillators. This is a striking segregation of the curve shapes. However, CaF_2:Eu is the exception preventing us from concluding that only activated alkali halides show such a hump. The NaI:Tl yield curve, for example, seems to represent the complexity of Eq. (25).

- A roll-off at low particle energy is common to all of the scintillators in both classes. Viewed in this way, the particle energy at which the roll-off occurs in each material is an important observation to be understood and to be fitted by a model attempting to describe the whole group of materials.

As given in Section 2 [Eqs. (1) - (2) and (8) - (11)], there are at least 14 rate constants and other physical parameters in the model that potentially influence the scintillation light yield. Given this large number of parameters, it is rather surprising that the existing data would follow such a simple pattern of almost rigid shift of each of two basic fixed shapes across the energy scale from material to material. It suggests that many of the 14 parameters may have very similar values through all the scintillating materials, i.e., fairly wide-gap dielectrics, and/or that relatively few of the parameters are responsible for the roll-off and hump. These hypotheses are to be explored through the calculations of yields to follow.

The above observations on appearance of the yield data suggest two problems to be tackled by a model attempting to account for the full range of data: (i) What is it that accounts for the "hump" in the yield for activated halides? (ii) Does the mainly rigid shift along the energy scale of the yield with otherwise nearly constant shape mean that only one or two physical parameters determine the main variation of non-proportionality from material to material?

3.1: NaI :Tl Scintillator

This is one of the most studied scintillating materials and hence many radiative and non-radiative rate constants and other parameters can be deduced from the experimental data on NaI:Tl.

These rates are considered first to calculate the local yield as a function of -*dE/dx* and total yield as a function of the particle's initial energy. These two types of calculated yields can be compared with the corresponding experimental yields plotted by Murray and Meyer [6] and Mengesha et al. [11] (see Fig. 1(b)), respectively.

The first parameter listed in Table I is R_{1x}, taken to represent the first-order radiative decay of the excited Tl^{+*} activator. Although the symbol R_{1x} defined in Section 2 refers to excitons, the intrinsic exciton luminescence contributes little to the light output of NaI:Tl doped to practical levels, and furthermore the self-trapped exciton has a lifetime shorter than Tl^{+*}. Thus almost all excitons and geminate e-h pairs that contribute through the Tl-activation channel should transfer their energy quickly to the activator, whose 1st order radiative decay is thereafter characteristic of the Tl^{+*} lifetime. This 1st-order lifetime has been measured under x-ray pulse excitation at room temperature by Blankespoor et al. [19] and has the observed value 170 ns, whose reciprocal gives the observed decay rate of 5.88 x 10^6 /s. The observed decay rate is the sum of R_{1x} and K_{1x}, the 1st-order radiative and nonradiative rates. The scintillator light yield of Na:Tl can be taken as approximately 45,000 photons/MeV. With a band gap E_g = 5.9 eV and $E_{eh} = 3E_g$ (requiring 17.7 eV per electron-hole pair), the quantum efficiency of NaI:Tl is thus about 80%. As an approximation, we will apply the 80% quantum yield criterion to each kinetic order separately. Thus the first order rates are required to satisfy $R_{1x}/(R_{1x} + K_{1x}) = 0.80$ and R_{obs} = 5.88 x 10^6 s^{-1} = R_{1x} + K_{1x}, which yields R_{1x} = 4.7x10^6 s^{-1} and K_{1x} = 1.2x10^6 s^{-1} as listed in Table I.

The next two rate constants in the table are R_{1eh} and K_{1eh}, the 1st-order radiative and nonradiative decay rates of e-h pairs. In treating 1st-order (geminate) recombination of electron-hole pairs we have to take account of a limitation of the present model formulation. The "exciton fraction" f_x was introduced to specify the fraction of Tl^{+*} activators that receive their energy from excitons, by which we mean geminately paired electron and hole. There is no fraction parameter

in the present model formulation to specify a limited subset of e-h pairs that decays geminately, apart from the population already designated as excitons. To associate a nonzero 1st-order radiative decay rate R_{1eh} with e-h pair decay in this model necessarily would mean that *all* e-h pairs decay with a 1st order rate. The data of Dietrich et al [20] shows that scintillation in NaI:Tl is dominantly a 2nd-order process of binary electron and hole capture on Tl^+ ions. In order to utilize the exciton fraction f_x to specify that only a limited subset of e-h pairs recombines geminately, we lump all geminate e-h radiative decay together with the 1st-order exciton term at the rate R_{1x} already discussed, and so formally set $R_{1eh} = 0$ to express that there is no 1st-order geminate radiative recombination outside the so-called exciton channel that is governed by the exciton fraction f_x.

We do not set $K_{1eh} = 0$ because the capture of either sign of charge carrier in deep traps represents a first-order removal process that can take carriers out of the electron-hole population during the detection gate width. We choose a somewhat arbitrary rate $K_{1eh} = 3 \times 10^6\ s^{-1}$ comparable to the value of R_{1x}. Since this is an arbitrary parameter, it will be held constant at the above value for all the four materials.

The time-dependence of NaI:Tl luminescence at room temperature following 420 keV electron pulse irradiation was measured over 6 decades of luminescence decay by Dietrich et al. [20]. The excitation density was 1×10^{17} e-h pairs/cm^3, determined by glass-block dosimetry and electron penetration depth at this energy. The data are fitted by a straight line of slope –2 on the plot of log luminescence versus log time scales. From the second order decay curve of this measurement, we can deduce $R_{2eh} = 3 \times 10^{-11}\ cm^3/s$ for the 2nd order radiative rate constant of non-geminate electron-hole recombination luminescence via Tl^+ activator ions.

To set an estimate of the nonradiative 2nd –order rate K_{2eh}, we go back to the 80% efficiency of total light yield from NaI:Tl, and again make the approximation of applying it separately in each kinetic order. Taking the 2nd and 3rd order losses together into account, a reasonable estimate of K_{2eh} consistent with the light yield considerations above is $K_{2eh} = 3 \times 10^{-12}\ cm^3/s$.

There is no known process in a doped scintillator like NaI:Tl that transfers energy to the activator through interaction of two excitons. Therefore the value of the 2nd order rate constant of "exciton" *radiative* decay can be set to zero, $R_{2x} = 0$. As noted earlier, in semiconductors where free exciton luminescence is dominant, exciton-exciton radiative collision processes (so-called p-band of luminescence) can accelerate radiative decay, but this is not typical of NaI:Tl or the other scintillators presently considered.

In contrast, exciton-exciton collisions and resonant interactions of close excitations even if immobilized on activator ions are well-known to be quenching mechanisms. One excitation can make a transition to the ground state while exciting a nearby exciton to a high-lying state which decays non-radiatively back to the lowest excited state or to the ground state. Its value is assigned as $K_{2x} = 2 \times 10^{-11}$ cm^3/s for NaI:Tl, which is close to the observed rates in semiconductors [21]. The bimolecular radiative recombination of this order of magnitude is also found in organic materials used for light-emitting diodes [22]

There is guidance on the free-carrier Auger recombination rate K_{3eh} from literature on various semiconductors. A value around $K_{3eh} = 1 \times 10^{-29}$ cm^6/s is typical. [23] Although in line with typical experimental values, the 3rd-order rate is only an estimate, so it is set to a single value constant for all the four materials considered here.

The exciton 3rd-order nonradiative rate K_{3x} is not considered to be very relevant in view of existence of the 2nd order nonradiative rate K_{2x}. We have therefore assigned it the same value as that of K_{3eh} and held it constant for all the four materials, i.e., $K_{3x} = 1 \times 10^{-29}$ cm^6/s.

The interchange rate of excitons converting into e-h pairs, may be given by:

$$\gamma_{xe} = \gamma_{ex} \exp(-\Delta E / kT), \qquad (27)$$

where the activation energy in NaI is taken to be $\Delta E = 0.06eV$ [24]. In this study we have considered three values of $\gamma_{eh-x} = 0$, $10^5 s^{-1}$ and $10^7 s^{-1}$ for NaI:Tl which from Eq. (27) give $\gamma_{xe} = 0$ and $9.86 \times 10^3 s^{-1}$ and 9.86×10^5, respectively, at 300 K. This is only to study the influence of γ_{eh-x} on the yield in NaI:Tl. Otherwise, for the other three scintillators, we have chosen $\gamma_{eh-x} = \gamma_{x-eh} = 0$. It may be noted that with the choice of rates given in table I, the temperature dependence appears in the yield only through the exchange rate γ_{xe}.

The track radius can be estimated to be about 4 nm (see the discussion in Sec. 4.3). This parameter has the simple effect of sliding a given curve left or right on the *dE/dx* scale, and approximately a similar effect of sliding the integrated light yield across the particle energy scale. A small track area means that a given *dE/dx* produces inversely proportionately higher excitation density n(x), which is the independent variable of this formalism. As noted above, the experimental data are quite remarkable in experiencing mainly a horizontal shift along the energy scale of curves that otherwise are mostly rigid in shape among two basic classes. NaI:Tl has its roll-off at the lowest energy (highest *dE/dx*), and so it should have the largest track radius. BaF_2 (core-valence) scintillation has its roll-off at the highest energy (lowest *dE/dx*), and there is good reason to expect that core holes will have negligible diffusion expanding the track. Thus we have considered the following track radii: NaI:Tl, $r = 6$ nm, BaF_2 (core/valence luminescence) $r = 2$ nm, GSO and $LaCl_3$:Ce $r = 4$ nm as given in Table I.

In addition to the above parameters, we also need the average ionization energy, *I,* and electron density ρ_e [Eq. (13)] for each material. For NaI, *I* is found to be 452.0 eV [25] and $\rho_e = 9.87 \times 10^{23}$ cm^{-3} from Eq. (13). Using the rates from Table 1 and 1st-order lifetimes defined

earlier as $\tau_{ex}^{-1} = R_{1x} + K_{1x}$ and $\tau_{eh}^{-1} = R_{1eh} + K_{1eh}$ one can calculate the coefficients a_1, a_2, a_3 and a_4 (from Eqs. (A.18) to A(21)) required for calculating the yield from Eqs. (8) and Eq. (11). The yields thus calculated and plotted are shown in Fig. 2(curve (1)) (local yield) and 3 (curve (1))(total yield) for NaI with $f_x = 0.1$. Results of Fig. (1) agree with the main qualitative shapes and placement on the energy axis of the experimental results of local [6] and total [11] (see Fig. 1(b)) yields for NaI:Tl.

For the other three materials considered, the parameters that we know differ significantly from NaI:Tl are the 1st order decay rate R_{1x}, and the corresponding nonradiative K_{1x} that can be deduced reasonably well from knowledge of the measured lifetime and absolute light yield efficiency All of the other 10 rates in Table I will be held at the same value for all the four materials.

3.2: BaF_2 (core-valence) Scintillator

The 1st - order rates can be estimated from the lifetime and total light yield of core-valence luminescence in BaF_2 [26] as $R_{1x} = 1.6 \times 10^9$ s^{-1} and $K_{1x} = 4.0 \times 10^8$ s^{-1}. The fast BaF_2 scintillator luminescence occurs due to core-valence transitions, where a Ba 5p shallow core hole is filled by an electron from the fluorine valence band. Because the valence electron concentration is so large, this rate depends only on the core hole concentration, i.e., is 1st order in excitation density. Hence we have set $f_x = 1$. Using the rates in table 2, $\rho_e = 1.20 \times 10^{24}$ cm^{-3}, $I = 180.4$ eV[25] and track radius of 2nm, the calculated local and total yields for BaF_2 are shown in Figs. 2(curve (2)) and 3 (curve (2)), respectively. These results reproduce the main qualitative features of the yield on the energy axis as seen in the experimental data [11] (see Fig. 1(a)).

3.3: Gd_2SiO_5:Ce (GSO) and $LaCl_3$:Ce Scintillators

The 1st-order radiative rate R_{1x} in cerium-doped materials GSO:Ce and $LaCl_3$:Ce is taken as 1/(30 ns). [27] These two scintillators have nearly identical luminescent properties and luminescence is

dominated by excitons, which means f_x is close to unity. The linear rate of excitonic radiative recombination is considered for present purposes to be dominated by its decay rate at the activator dopant Ce^{3+} and is thus assigned the radiative rate $R_{1x} = 3.00 \times 10^7$ s^{-1}[27]. Although Gd^{3+} may contribute to the luminescence in GSO:Ce through its f levels, the radiative rate of f-f transitions would be significantly lower than for the Ce^{3+} 5d-4f transition. The linear exciton and e-h pair quenching rates are assumed to be one order of magnitude less than this, i.e., $K_{1x} = K_{1eh} = 3x10^6$ s^{-1} and $R_{1eh} = 0.0$.

We have used the track radius of 4 nm for both the crystals. $\rho_e = 1.16 \times 10^{24}$ cm^{-3} and I = 329.5 eV[25] are used for $LaCl_3$:Ce. $\rho_e = 1.92 \times 10^{24}$ cm^{-3} and I = 170.1 eV[25] are used for GSO. Using the rates from Table I and these values for ρ_e and I, the calculated yields are plotted in Fig. 2 (curve (3)) and Fig. 3 (curve (3)) for GSO with f_x = 1 and in Fig. 2 (curve (4)) and Fig. 3 (curve (4)) for $LaCl_3$:Ce with f_x = 0.6. These yields reproduce the main qualitative shape and general ordering on the energy axis as seen in the experimental data. [11, 28].

4. Discussions

4.1 Discussions of results of analytical model

A phenomenological approach is applied within the first order approximation to derive an expression for the light yield from a scintillating crystal as a function of the initial deposited energy $(-\frac{dE}{dx})$ at each point on the track as well as the total initial energy, E, deposited in the whole track of a gamma ray. It is considered that the deposited incident γ -ray energy along its track excites high density of e-h pairs, some of which may form excitons. Such excitons and independent electrons and holes may go through several radiative and non-radiative interaction processes during their lifetime. Here we have considered only linear, binary and ternary radiative and non-radiative processes and their rates of radiative and non-radiative (quenching)

recombinations are taken into account in the rate equations (1) and (2). Accordingly the approximate expressions for the local and scintillation light yields derived in Eqs.(8) and (11) are functions of all these three types of rates of recombination. It is assumed that the ternary (Auger) recombination can only occur non-radiatively.

For the calculation of yields in these scintillators, the relevant rates are taken into account and the estimation of their magnitudes is based on the experimental results. In estimating the binary and ternary rates, guidance from the experimental results in semiconductors is also taken. The calculated local yield rises first to a maximum and then starts decreasing at higher locally deposited energies for materials that have mixed or dominantly e-h excited pairs, for example NaI:Tl with f_x = 0.1 shown in Figs. 2(curve (1)) and 3 (curve (1)) and $LaCl_3$:Ce with f_x = 0.6 in Figs. 2(curve (4)) and 3 (curve (4)). Scintillators operating dominantly on excitonic luminescence (f_x = 1) do not exhibit such a rise in the local yield see, for example, BaF_2 and GSO shown in Figs. 2 and 3 (curves (2) and (3)) . Also $LaCl_3$:Ce becomes dominantly excitonic for f_x > 0.6 and then the hump disappears. The behaviour of the total yield has the opposite character because of the reciprocal relationship between the local energy -*dE/dx* and total energy *E* as given in Eq. (12). Such a dependence of the total yield on total energy agrees reasonably well with the experimental results of Mengesha et al. [11] (see Fig. 1).

From the calculated yield, shown in Figs. 2 - 3 for NaI:Tl, BaF_2, GSO and $LaCl_3$:Ce , it is found that the rates of linear processes (R_1 and K_1) play a dominant role initially at low values of $(-\frac{dE}{dx})$. In the middle range values of $(-\frac{dE}{dx})$, the rates of binary process (R_2 and K_2) play important roles and K_3 becomes important only in the very high energy range. This is obviously what one would expect because at the lower deposited energy the excitation density is low and interactions among excitons and e-h pairs will be weak so only linear processes will be dominantly

effective. As the deposited energy increases, the excitation density increases and interactions among excitations (excitons and binary e & h) become stronger and stronger and therefore the binary rates become important in the middle to high energy range and ternary rate becomes significant at very high deposited energies when the excitation density becomes largest. A similar dependence on different rates can be interpreted from the total yield (Eq. (11)) plotted as a function of E. The yield dependence on the total gamma ray energy, E, depends theoretically on the form of (*-dE/dx*) chosen for the relation between these two quantities because the Bethe equation [Eq. (12)] appears in the literature in a few different forms [8, 29]. The form used here given in Eq. (12) requires two material dependent parameters, ionization energy *I* and electron density ρ_e. However, as the range of energy is quite high the reciprocal relationship between local and total yield dominates [8].

The effect of the interchange rates γ_{ex} and γ_{xe} on the local and total yields are shown for NaI:Tl in Fig. 4 (a) and (b), respectively, for $\gamma_{ex} = 10^5$ s^{-1} ($\gamma_{xe} = 9.86\text{x}10^3$ s^{-1}) and 10^7 s^{-1} ($9.86\text{x}10^5$ s^{-1}). These values are chosen due to the fact that according to Eqs. (A.6) and (A.7) if, on one hand, γ_{ex} is less than 10^4s^{-1}, i.e., much less than $R_{1x}+K_{1x}$ and $R_{1eh}+K_{1eh}$, it has negligible effect on both local and total yields. On the other hand if γ_{ex} is much larger than $R_{1x}+K_{1x}$ and $R_{1eh}+K_{1eh}$ then the material shows dominantly only the excitonic character (see the dotted yields in Figs. 4(a) and (b)).

It may be noted that the initial excitation density at position *x* along the track, *n*(*x*) [Eq. (3)] is the independent variable in the local yield [Eq. (8)] in this model. After the constants $a_1 - a_4$ are determined, the shape of the light yield curve versus *n*(*x*) is entirely determined. However, comparisons to available experiments are represented either in the form of the local yield versus -*dE/dx* [6], or more directly as total yield versus initial electron energy [8, 11, 30], but not as the

light yield versus $n(x)$. According to Eq. (3), $-dE/dx$ is related to $n(x)$ as the square of the track radius during light emission. This factor produces a rigid shift of the local light yield curve along the horizontal axis without changing its shape. To obtain the comparison with the total yield versus initial electron energy, we have integrated the local light yield versus $-dE/dx$ along the whole track. Because of this step, the integrated light yield curves will not be perfectly rigid in shifting with changing track area, but since all of the component curves versus $-dE/dx$ shift rigidly, the integrated light yield can be expected to qualitatively resemble a rigid shift along the horizontal (energy) axis as the track area changes. With at least 14 parameters contributing in principle to the light yield curves in this model, it seems unlikely that they would change in an orchestrated way so as to produce a rigid shift along the energy axis from material to material. Of all those 14 parameters, track radius is the one having the most obvious tendency to produce a nearly rigid shift along the energy axis.

One of the important points in determining the shape of the light yield is also the fractional excitonic concentration, f_x. As stated in section 3, if the excitonic concentration is dominant, $f_x \to 1$, the hump in the yield disappears as it is found in the case of $LaCl_3$:Ce for $f_x >$ 0.6. It may therefore be important to understand how in some materials there are more excitons, e.g., BaF_2 and GSO, and in others there are more e-h pairs. This depends on how both carriers diffuse along the track radius after the initial excitations. To discuss this point further, the case of NaI:Tl is discussed below.

4.2 Estimation of track radius: Consideration of carrier diffusion in NaI:Tl

Without yet considering any internal electric fields, the mean distance that an electron or hole can travel from its point of origin within a time t is $\langle r \rangle = \sqrt{Dt}$ [31] where the electron (hole) diffusion coefficient D is related to the electron (hole) mobility μ by the Einstein formula, $\mu = \frac{eD}{k_B T}$.

The conduction electron mobility has been measured in KI as $\mu_e = 20$ cm^2/Vs at room temperature [32]. The mobility becomes much larger at low temperature and depends on sample purity. In CsI, Aduev et al [33] have measured $\mu_e = 8$ cm^2/Vs at room temperature by electron pulse-induced conductivity. Since NaI:Tl has rather high Tl doping, it's electron mobility will not be expected to be as high 20 cm^2/Vs. If it is near 8 cm^2/Vs, then at room temperature, $D = 0.21$ cm^2/s and considering only the electrons, the mean displacement would be about 4.6 nm in 1 ps, and 145nm in 1 ns. Based on their effective mass, the free holes may be expected to have roughly 1/8 the mobility of electrons (1 cm^2/Vs) before self-trapping.. Furthermore, the time of free hole diffusion in the valence band before self-trapping is about 1 ps. So the corresponding mean displacement due to diffusion of free holes before self-trapping would be about 1.6 nm from the origin established in the initial distribution. Were we to demand a zero internal electric field, the slower hole diffusion and eventual self-trapping of holes would confine the distribution of both electrons and holes at the smaller displacement value.

Now compare this situation to diffusion of conduction electrons from an n-type semiconductor into an intrinsic region or a p-type region. In the central track of the scintillator, and on a time scale shorter than completion of recombination luminescence ($<<$ 1 μs) it is useful to identify a pseudo-Fermi level for the dense population of conduction electrons excited. On the nonequilibrium time scale which is comparable to the time for radiative recombination of electrons and holes across the gap, the relatively immobile holes can be viewed in the electrostatic role of ionized donors in our semiconductor analogy. That is, if some electrons diffuse across the cylindrical boundary of the initially excited track core into the surrounding unexcited crystal, the holes left behind will set up a charge depletion region whose electrostatic potential will eventually limit further diffusion of electrons into the unexcited region. The highest yield in NaI:Tl is observed at an energy of 10 keV[see Fig. 1(b)] . Using this in eq. (14) for a 6 nm track radius we get $n(x) = 10^{18}$ excitations/cm^3. Using then Fick's law, $J_N = -D\nabla(N)$, we get a diffusion current

so large that the field-balanced electron distribution should be established within some tens of picoseconds at most.

At that point in time the electrons will have diffused out ahead of the holes to a mean radius determined by the internal electric field. We presume that the holes are self-trapped and are thus essentially immobile on the time scale longer than a picosecond. Since the NaI scintillator is Tl-doped to typically 0.3%, we can further presume that the electrons after fast diffusion will have become trapped at their forward positions on Tl^+ ions to form Tl^0. This is slightly different from the p-n junction analog, in which the electrons having diffused into the p-type region as minority carriers are in equilibrium with the acceptors [31], but the analogy remains good in the following way that identifies what the "built-in potential" that limits further diffusion should be. Within the excited central 2-nm track core during the nonequilibrium condition, the pseudo Fermi level (applying to conduction electrons only) should be very close to the conduction band edge at an electron density of $n(x) = 10^{18}$ excitations/cm^3 (electron = hole = excitation density). In the initially unexcited crystal outside the central core, the Fermi level for electrons captured on Tl^0 states of activators should be at about the energy of the Tl^0 charge state, i.e. approximately 0.3 eV below the conduction band edge [20]. The built-in potential difference at the boundary between the two depletion regions (inside and outside the initially excited core) should therefore also be about 0.3 eV.

The electron diffusion will finally be balanced by the built-in depletion layer field (in the radial geometry of the track), within a time we have assumed to be tens of picoseconds, but the scintillation light output occurs on the hundreds of nanoseconds up to a microsecond time scale. It has already been shown in various publications [20, 34-35] that hopping transport of self-trapped holes occurs on the time scale of the scintillation light pulse. Thus our outlined process would be completed when the self-trapped holes hop outward from the track core to recombine radiatively

with Tl^0 at the periphery and/or to be trapped as Tl^{++} and recombined with an electron thermally released from Tl^0.

A very good model for the electrostatics of this situation is the cylindrical capacitor. The initially excited core with possible limited diffusion of holes before self-trapping is modelled as the inner cylinder of the capacitor having a radius of 6 nm and carrying a total positive charge density corresponding to an unbalanced hole concentration of 10^{18} holes/cm^3. We consider that these holes remain stationary but that the electrons of equal number initially occupying the same cylinder volume move outward to occupy an outer cylindrical shell of radius *b*. The interior radius already assigned as 6 nm may be denoted as *a*. The linear charge density of both the positively and negatively charged shells described above is: $\lambda = (10^{18}\ \text{holes/cm}^3)(\pi r^2) = 2 \times 10^{-11}$ Coul/m.

A cylindrical capacitor of inner radius *a,* outer radius *b*, and the linear +/- charge densities λ, has a voltage difference *V* between the inner and outer cylinders $V = \frac{\lambda}{2\pi\varepsilon\,\varepsilon_0}\ln\frac{b}{a}$ [36]. In NaI, ε = 6.6. Assuming that the outer radius is ten times larger than the inner radius, we find $V = 0.125$ V for the outer shell (electrons) of radius $b = 60$ nm. This is smaller than the built-in potential of 0.3 V described above. Therefore we may conclude that 60 nm is not a large distance for the diffusing electrons to run ahead of the more immobile holes. This creates an initial charge separation which prevents initial exciton formation in NaI:Tl and promotes eventual diffusive recombination of separated electrons (trapped on Tl^0) and holes (either self-trapped or on Tl^{++}). This diffusive stage may be sensitive to other crystal impurities and defects, and should be examined with respect to observed impurity and defect effects on the light yield curves.

Thus, diffusion forces the mobile electrons to move very quickly out beyond the relatively immobile holes, discouraging formation of excitons. This rapid diffusion stage sets up two separated charge reservoirs (holes near the core, electrons farther out), which necessarily must recombine as independent electrons and holes (generally with one or both trapped on thallium by the time of recombination). Finally, the self-trapping of holes may make itself felt in determining "hump or no hump" in the plot of scintillation yield vs E (Fig. 1), and also the ability of Tl to trap both charges independently plays a role. If it were not for self-trapping of the holes, they would tend to diffuse out pretty far along with the electrons, and furthermore if the electrons were not trapped by the Tl^+ to form Tl^0, those holes would catch up to free electrons and form excitons. From then on, the kinetics would be first order and will give rise to no hump. Thus, the above discussions for NaI:Tl provide insight of why excitonic radiative recombination may be relatively unimportant in this material and justifies the assumption of low excitonic fraction $f_x = 0.1$.

In contrast, the case of the shallow core holes in BaF_2 gives rise to core-valence luminescence. The core hole mobility should be very small, and the electrons recombining with the core holes are in this case plentiful valence electrons for which diffusion plays no significant role in the kinetics. Thus, BaF_2 may be assigned with the negligible diffusion effect and hence the track radius is chosen to be 2 nm (Table I). The core hole decay rate is 1^{st} order because the recombination partners are dense valence electrons, and hence $f_x = 1$ is chosen for this material and the calculated yield agrees reasonably well with the observed yield. The cases of GSO and $LaCl_3$ may be considered to be midway between BaF_2 and NaI:Tl and hence the track radius is assumed to be 4 nm. In both of these cases the excitonic radiative recombination is assumed to be significant. For GSO:Ce, the calculated scintillation yield agrees reasonably well with the experimental yield vs E for $f_x = 1$ without any hump. However, for $LaCl_3$:Ce the calculated light yield curve represents the experimental one quite well with $f_x = 0.6$. The hump disappears at $f_x > 0.6$. It is not possible to

analyse the results of BaF_2, GSO and $LaCl_3$ beyond these qualitative trends in shape of the yield curve at this stage without more supporting experimental works on the rate constants.

One may wonder why the response of a scintillator like YAP, which shows a proportional light yield (see Fig. 1(a)), has not been considered in this paper? In view of the influences of various orders of rates of radiative and non-radiative processes presented here, the case of YAP may be considered as a special case of being pure excitonic ($f_x = 1$) presented in section 2.4 with higher order rates being negligibly small , i.e. R_{nx} , $K_{nx} << R_{1x,} K_{1x}$ ($n > 1$). In this case the light yield becomes nearly constant $\approx a_1$ (see Eqs. (8), (11) and (23)).

4.3 Additional comments on the axial and radial distribution of excitations in the track region

In this section we will try to justify our model of the cylindrical track and make some estimations of the radial and axial distribution of electronic excitations based on the detailed discussion of elementary scattering processes for high-energy charge carriers.

The spatial distribution of excitons, electrons and holes (electronic excitations, EEs) after the interaction of the primary electron with matter is formed during all stages of the creation/relaxation processes. In the Born approximation these processes can be regarded as sequential scattering events with emission and absorption of real and virtual photons and phonons. At each scattering event the primary electron loses an energy $\hbar\omega$ and momentum $\hbar\mathbf{q}$. The energy losses can be described in the polarization approximation and non-relativistic limit as:

$$-\frac{dE}{dx} = \frac{2}{\pi a_B m v^2}\int_0^E \hbar\omega\, d(\hbar\omega)\int_{q_-}^{q_+}\frac{dq}{q}\,\mathrm{Im}\left(-\frac{1}{\varepsilon(\omega,q)} - \frac{2}{\varepsilon(\omega,q) - c^2q^2\ \omega^2}\right), \qquad (28)$$

where $\hbar q_+$ and $\hbar q_-$ are maximal and minimal momentum transfers, respectively, $\hbar q_\pm = \sqrt{2m}\left(\sqrt{E} \pm \sqrt{E-\hbar\omega}\right)$, E is the electron kinetic energy, v is its velocity, and a_B is the Bohr radius. The first term in brackets in Eq. (28) corresponds to emission of virtual longitudinal photons, which are instantly absorbed by the media. In insulators the energy loss function

$\mathrm{Im}\left(-\varepsilon^{-1}(\omega,q)\right)$ is non-zero in two regions: (1) if $\hbar\omega$ is greater than the minimal energy of the creation of an electronic excitation (band gap energy E_g or free exciton energy E_{ex}), then the absorption of the virtual photon by the media results in the creation of additional electronic excitations. (2) when $\hbar\omega$ is about equal to the lattice phonon frequencies; the corresponding scattering process describes the elementary act of the cooling of an electron without creation of additional electronic excitations, i.e., the thermalization of electronic excitations. For $\hbar\omega \approx k_B T$ (T is the crystal temperature) Eq. (28) needs to be modified in order to account for the processes of stimulated phonon emission and absorption. The second term in brackets in Eq. (28) corresponds to emission of real transverse photons (e.g., bremsstrahlung).

In order to obtain the electron stopping power $-dE/dx$ in this section, we use a modified form [29, 30], which helps us to estimate the stopping power in a wide energy range from several eV to 1 MeV. We discuss here the structure of the energy loss function in the fundamental absorption region considering NaI crystal as an example. The calculation of the energy loss function $\mathrm{Im}\left(-\varepsilon^{-1}(\omega,q)\right)$ can be performed by following the steps described below:

(1) First we calculate $\mathrm{Im}\left(-\varepsilon^{-1}(\omega,0)\right)$. Here $\varepsilon(\omega,0)$ is calculated using the Evaluated Photon Data Library (EPDL97) data bases [37] developed at the Lawrence Livermore National Laboratory. For the case of ionic crystals, this requires the following corrections: (i) Modify the ionization energies of elements using the rigid shift of core level positions in order to obtain the correct ionization energies of shallow shells (a kind of the account for Madelung crystal potential), and (ii) change the population of the outer shells (e.g. for NaI we use the pure ionic model Na^+I^- with 6 electrons at 5*p* iodine valence shell and zero electrons at 3*s* sodium shell). The partial photon absorption cross-sections obtained from EPDL97 library are summed in order to obtain the imaginary part of dielectric permittivity $\varepsilon_2(\omega,0)$.

(2) The real part $\varepsilon_1(\omega,0)$ of $\varepsilon(\omega,0)$ is reconstructed using the Kramers-Krönig procedure. Then both $\varepsilon_2(\omega,0)$ and $\mathrm{Im}(-\varepsilon^{-1}(\omega,0))$ functions are checked using the sum rules for the total number of electrons per unit crystal cell and for the value of low-frequency dielectric permittivity. Thus, we check that the resulting energy loss function shows the plasmon peak at the correct energy, and its intensity is also realistic.

(3) Then we extrapolate the energy loss function for the case of non-zero **q**. This method is equivalent to using the Generalized Oscillator Strength (GOS) approximation instead of Optical Oscillator Strength (OOS) approximation [12-13]. We use the procedure based on the plane wave approximation of the final electron state. The results thus obtained for NaI are presented in Fig. 5.

Let us discuss the details of this electron loss function. First of all we introduce the variable $E_q = \hbar^2 q^2 / 2m$ instead of q. In this case the limits of integration over this variable becomes $\left(\sqrt{E} \pm \sqrt{E-\hbar\omega}\right)^2$. The maximal value of the upper integration limit E_q^+ equals to $4E$ (for $\hbar\omega = 0$). From simple kinematics considerations this case corresponds to the back scattering of the primary electron from the massive scattering center at $\mathbf{q} = -2\mathbf{p}$, and in this case the scattering angle is π. When $E_q \approx E$, the mean scattering angle for primary electron is about $\pi/2$. The scattering angle is small if $E_q << E$.

For high electron energies $E > 1$ keV, most scattering events occur for small E_q due to two reasons: (1) the factor $1/q$ in the integrand makes q small and therefore small E_q is more preferable for scattering and (2) Fig. 5 (lower panel) shows that the energy loss function rapidly decreases with increasing E_q. Therefore the primary electron trajectory deviates slightly at each scattering. The occurrence of scatterings with higher angular deviations of the trajectory is relatively rare. The Bethe ridge (see, e.g., [12]) of the energy loss function plays an important role

in these rare scattering events. The Bethe ridge is the peak in the energy loss function near the line $\hbar\omega = E_q$. It is clearly shown in the bottom panel of Fig. 5 and describes the Rutherford scattering (or Mott scattering, if the exchange is taken into account) of the primary electron by quasi-free electrons. This scattering is the main reason of the creation of so-called δ -rays. An additional reason for the creation of δ -rays is the creation of high-energy Auger electrons followed after the ionization of K- and L-shells of heavy ions. This is again rather a rare process, as it can be seen from the energy loss function presented in Fig. 5. These K- and L-shells can be filled also with the X-ray fluorescent photon emission, and the absorption of these photons creates high-energy electrons far enough from the main track. The creations of both deep core holes and δ -rays are relatively rare effects, therefore the main part of energy is deposited in the crystal in the form of sequential low-angle scattering of the primary electron.

The scattering of electrons with energies below 100 eV is mainly a large-angle scattering, and these electrons produce a 'cluster' of excitations sometimes called 'spurs', see, e.g., [38].

For the relativistic case, the following modifications should be made in Eq. (28). The factor $mv^2\ 2$, which is equal to kinetic energy E in non-relativistic case should be replaced by $\frac{mv^2}{2} = E\frac{2 + E/mc^2}{2\left(1 + E/mc^2\right)}$ and then the limits of the integration are changed to:

$$\begin{aligned}\hbar q_{\pm} &= p(E) \pm p(E - \hbar\omega) = c^{-1}\sqrt{\left(E + mc^2\right)^2 - m^2c^4} \pm c^{-1}\sqrt{\left(E - \hbar\omega + mc^2\right)^2 - m^2c^4} \\ &= \sqrt{E\left(E + 2mc^2\right)} \pm \sqrt{(E - \hbar\omega)\left(E - \hbar\omega + 2mc^2\right)}.\end{aligned} \tag{29}$$

The exchange of indistinguishable electrons is not included in this form of the stopping power. However this effect modifies the stopping power only when the energies of the secondary electrons and scattered primary electrons are about the same, i.e., the exchange modifies mainly the low-energy part (below the mean ionization energy) of the stopping power and the decrease is no more than by a factor of two.

For the first step, as an approximation, when the q-dependence of dielectric permittivity is neglected we get: $\mathrm{Im}\left(-\varepsilon^{-1}(\omega,q)\right)\approx \mathrm{Im}\left(-\varepsilon^{-1}(\omega,0)\right)$. In this case we neglect the effects connected with the Bethe ridge (see, e.g., [12]), i.e., neglect the large-angle scattering on quasi-free electrons, which is expected to overestimate the stopping power slightly. The stopping power is then calculated using:

$$-\frac{dE}{dx}=\frac{1}{\pi a_B E}\frac{2\left(1+E/mc^2\right)^2}{2+E/mc^2}\int_0^E \hbar\omega\, d(\hbar\omega)\,\mathrm{Im}\left(-\frac{1}{\varepsilon(\omega,0)}\right)\times\ln\frac{\sqrt{E}\sqrt{E+2mc^2}+\sqrt{E-\hbar\omega}\sqrt{E+2mc^2-\hbar\omega}}{\sqrt{E}\sqrt{E+2mc^2}-\sqrt{E-\hbar\omega}\sqrt{E+2mc^2-\hbar\omega}}. \quad (30)$$

The electron stopping power calculated with this technique for sodium iodide (NaI) is shown in the top panel of Fig. 6 (left y-axis). Electrons with energy below 80 eV are scattered with production of electronic excitations mainly from the valence band, whereas electrons with higher energy create holes in iodine 4*d* core level (ionization energy is about 60 eV) and deeper levels.

The mean free path for electron-electron scattering and mean energy losses per a scattering versus electron energy are shown in the bottom panel of Fig 6. The mean energy per one scattering is about 70 eV for primary electron energy in the range 100 keV to 1 MeV. Therefore most scatterings produce secondary excitations originating from the valence I 5*p*, Na 2*p* and I 4*d* bands. Assuming that the mean energy for production of an electronic excitation E_{eh} can be estimated as 2 to 3 times the band gap energy E_g (5.9 eV for NaI), one can estimate that in the high-energy part of the track, individual scatterings produce clusters ('spurs') of relaxed tertiary electronic excitations. The number of electronic excitations in these clusters is about 3 to 5.

The mean radius of these clusters is determined mainly by the thermalization length. Since the main channel for thermalization of electrons and holes in ionic crystals is the scattering on LO and short-wavelength LA phonons, the mean radius of the cluster can be estimated as r_{th} = 3 nm. This value is too hard to be estimated accurately, since the main role in the thermalization process

is played by the short-wavelength LA phonons with wavevectors near the boundary of the Brillouin zone. This interaction is especially strong and therefore the thermalization length is shorter in binary crystals with high ionic degree, and in crystals with ferroelectric features.

For estimating the radius of these clusters, we have to take into account not only the thermalization length, but also the diffusion length for thermalized excitations before their capture by traps or self-trapping. As stated in section 4.2, the hole mobility for alkali halides is about 1 $cm^2/V{\cdot}s$, which gives a diffusion coefficient $D = 2.6{\cdot}10^{-2}$ cm^2/s at $T = 300K$ (see section 4.2). As described above, the mean distance which a charge carrier can go away during time t from the place of its creation is $r_D = \sqrt{Dt}$, which gives $r_D = 6$ nm in 1 ps and 50 nm in 1 ns. Assuming that the self-trapping or capturing occurs in few picoseconds, we get the mean distance of the travelling before the capture equal to 3 nm in 4 ps. Therefore the total mean distance from the creation to trapping of a hole can be estimated as $r = \sqrt{r_{th}^2 + r_D^2} \approx 4\,\text{nm}$. The trapping on impurities depends on their concentration and therefore r can be different in the same matrices with different dopant concentrations.

The value of r can hardly be measured directly. Nevertheless, the analysis of decay curve profile of BaF_2 cross-luminescence excited under 20 to 100 eV photons [39] gives the indication that the radius of the 'clusters' is about several nanometers [40].

According to the mean free path plot shown in the bottom panel of Fig. 6, these clusters are separated by the mean distance of about 50 nm at the high-energy part of the track and overlap at the low-energy end of the track below 10 eV. This structure of the track is rather complicated, and for simplicity we propose a model which replaces the real distribution of electronic excitations by a Gaussian distribution in the transversal direction with mean radius r and peak concentration at the track axis equal to $n_{\max}(x) = (-dE/dx)/(\pi r^2 E_{eh}) \approx (-dE/dx)/(3\pi r^2 E_g)$ as given in Eq. (9) and:

$$n(\mathbf{r},0) \equiv n(x,\tilde{\mathbf{n}},0) = n_{\max}(x)\exp\left(-\tilde{\mathbf{n}}^2/r^2\right), \text{ where } 0 \le \rho \le r. \quad (31)$$

Since $n_{\max}$ is proportional to $-dE\ dx$, it can be estimated as shown in the top panel of Fig. 6 (right y-axis).

In the previous sections we have used the model of the cylindrical track with the stepwise radial distribution of electronic excitations. The estimation presented in this section justifies the applicability of the cylindrical track model and the values of track radius given in Table I which have been used in Sec. 3 for the analytical calculation of the non-proportionality effect.

5. Conclusion

A phenomenological approach is applied to derive an approximate expression for the light yield in scintillators as a function of the rates of linear, binary and ternary radiative and non-radiative interaction processes. The dependence of the light yield on the initial energy deposited at any point along the γ - ray track (-dE/dx) and the total energy (E) deposited in the whole track is studied. The calculated yield is found to be in reasonable agreement with the yield observed in scintillators. The energy and radial dependences on the excitation concentration along the track are also discussed. It is expected that the results of this paper may enhance understanding of the dependence of the light yield on different rates of radiative and non-radiative interaction processes occurring in scintillators.

Acknowledgements

This work was supported by the National Nuclear Security Administration, Office of Defense Nuclear Nonproliferation, Office of Nuclear Nonproliferation Research and Engineering (NA-22) of the U.S. Department of Energy under Contract No. DE-AC02-05CH11231, grant number NNSA LB06-316-PD05 / NN2001000. We gratefully acknowledge the technical assistance from Ms Francesca Morlino in preparing the manuscript. We would like to thank Steve Payne of Lawrence

Livermore National Laboratory for sharing his own comprehensive framework prior to publication in terms of describing nonproportionality of scintillators.

Appendix A: Derivation of the excitation population

As an approximation, we consider only the linear processes in Eqs. (4) and (5) and then these equations become:

$$(R_{1x} + K_{1x}) < n_{ex}(x) > + \gamma_{xe} < n_{ex}(x) >= \gamma_{ex} < n_{eh}(x) > + f_x n(x), \quad \text{(A.1)}$$

$$(R_{1eh} + K_{1eh}) < n_{eh}(x) > + \gamma_{ex} < n_{eh}(x) >= \gamma_{xe} < n_{ex}(x) > + (1 - f_x) n(x), \quad \text{(A.2)}$$

Adding (A.1) and (A.2), we get:

$$(R_{1x} + K_{1x}) < n_{ex}(x) > + (R_{1eh} + K_{1eh}) < n_{eh}(x) >= n(x), \quad \text{(A.3)}$$

Solving the linear Eqs (A.1) and (A.2) using Eq. (A.3), we get :

$$< n_{ex}(x) >= An(x) \quad \text{and} \quad < n_{eh}(x) >= Bn(x) \ , \quad \text{(A.4)}$$

where

$$A = \frac{[\gamma_{ex} + (R_{1eh} + K_{1eh}) f_x]}{(R_{1x} + K_{1x})(R_{1eh} + K_{1eh}) + \gamma_{ex}(R_{1x} + K_{1x}) + \gamma_{xe}(R_{1eh} + K_{1eh})} \ , \quad \text{(A.6)}$$

and

$$B = \frac{[(1-f_x)(R_{1x}+K_{1x})+\gamma_{xe}]}{(R_{1x}+K_{1x})(R_{1eh}+K_{1eh})+\gamma_{ex}(R_{1x}+K_{1x})+\gamma_{xe}(R_{1eh}+K_{1eh})} \quad . \qquad \text{(A.7)}$$

We also need $< n_{ex}^2(x) >$, $< n_{eh}^2(x) >$ and $< n_{eh}^3(x) >$, which can also be determined from the linear order approximation, within which the concentration can be assumed to have the following form:

$$n_{ex}(x) = n_{ex}^0(x)e^{-t/\tau_{ex}} \ , \quad 1/\tau_{ex} = R_{1x} + K_{1x} \ , \qquad \text{(A.8)}$$

and $$n_{eh}^0(x,t) = n_{eh}^0(x)e^{-t/\tau_{eh}} \ , \quad 1/\tau_{eh} = R_{1eh} + K_{1eh} \ , \qquad \text{(A.9)}$$

where τ_{ex} and τ_{eh} are lifetimes of an exciton and an e-h pair, respectively. The above form assumes that the initial population of excitons and e-h pairs created at any point x decays exponentially in time through the linear processes. The advantage of the forms in Eqs. (A.8) and (A.9) is that these can be integrated on time easily and then we get:

$$< n_{ex}(x,t) >= n_x^0(x)\int_0^\infty e^{-t/\tau_{ex}}\,dt = n_{ex}^0(x)\tau_{ex} \, , \qquad \text{(A.10)}$$

and

$$< n_{eh}(x,t) >= n_{eh}^0(x)\int_0^\infty e^{-t/\tau_{eh}}\,dt = n_{eh}^0(x)\tau_{eh} \ . \qquad \text{(A.11)}$$

We also get:

$$< n_{ex}(x,t)^2 >= n_{ex}^0(x)^2 \int_0^\infty e^{-2t/\tau_{ex}}\, dt = \frac{1}{2} n_{ex}^0(x)^2 \tau_{ex}, \qquad \text{(A.12)}$$

$$< n_{eh}(x,t)^2 >= n_{eh}^0(x)^2 \int_0^\infty e^{-2t/\tau_{eh}}\, dt = \frac{1}{2} n_{eh}^0(x)^2 \tau_{eh}, \qquad \text{(A.13)}$$

and

$$< n_{eh}(x,t)^3 >= n_{eh}^0(x)^3 \int_0^\infty e^{-3t/\tau_{eh}}\, dt = \frac{1}{3} n_{eh}^0(x)^3 \tau_{eh}. \qquad \text{(A.14)}$$

Using Eqs. (A.10) and (A.11) in Eq. (A.4), we get:

$$n_{ex}^0 = A\, n(x)/\tau_{ex}, \quad \text{and} \quad n_{eh}^0 = B\, n(x)/\tau_{eh}. \qquad \text{(A.15)}$$

Using Eqs. (A.10) to (A.15) in Eq. (7), the light yield can be expressed as:

$$Y = \frac{(R_{1x}A + R_{1eh}B)n(x) + (\frac{1}{2\tau_x} R_{2x}A^2 + \frac{1}{2\tau_{eh}} R_{2eh}B^2)n(x)^2}{[((R_{1x}+K_{1x})A + (R_{1eh}+K_{1eh})B)n(x) + (\frac{1}{2\tau_x}(R_{2x}+K_{2x})A^2 + \frac{1}{2\tau_{eh}}(R_{2eh}+K_{2eh})B^2)\, n(x)^2 + (\frac{1}{3\tau_x^2} K_{3x}A^3 + \frac{1}{3\tau_{eh}^2} K_{3eh}B^3)n(x)^3]} \qquad \text{(A.16)}$$

Dividing the numerator and denominator of Eq. (A.16) by, $(R_{1x} + K_{1x})A\,n(x) + (R_{1eh} + K_{1eh})B\,n(x)$, we can write Y in the following form:

$$Y = \frac{a_1 + a_2 n(x)}{1 + a_3 n(x) + a_4 n(x)^2}, \tag{A.17}$$

$$a_1 = \frac{(R_{1x}A + R_{1eh}B)}{D}; \qquad D = (R_{1x} + K_{1x})A + (R_{1eh} + K_{1eh})B, \tag{A.18}$$

$$a_2 = \frac{(R_{2x}A^2/\tau_x + R_{2eh}B^2/\tau_{eh})}{2D}, \tag{A.19}$$

$$a_3 = \frac{(R_{2x} + K_{2x})A^2/\tau_x + ((R_{2eh} + K_{2eh})B^2/\tau_{eh}}{2D}, \tag{A.20}$$

$$a_4 = \frac{1}{3D}\left(\frac{K_{3x}A^3}{\tau_x^2} + \frac{K_{3eh}B^3}{\tau_{eh}^2}\right). \tag{A.21}$$

References

[1] W. W. Moses, S. A. Payne, W.-S. Choong, G. Hull, and B. W. Reutter, IEEE Trans. Nucl. Science IEEE Trans. Nucl. Sci. **55,** 1049 (2008) .

[2] W. W. Moses, Proc. International Conference on Inorganic Scintillators and their Applications, SCINT'99, Eds. V. Mikhailim, Moscow, Russia, 1999.

[3] E. R. Siciliano, J. H. Ely, R. T. Kouzes, B. D. Milbrath, J. E. Scheppe and D.C. Stromswold, Nucl. Instr. Methods in Physics Research A **550**, 647 (2005).

[4] M. Globus, B. Grinyov and J. K. Kim, *Inorganic Scintillators for Modern and Traditional Applications* (Institute for Single Crystals, Kharkov, Ukraine, 2005)

[5] See, e.g., J.D. Valentine, B.D. Rooney and P. Dorenbos, IEEE Trans. Nucl. Science **45**, 1750 (1998).

[6] R.B.Murray and A. Meyer, Phys. Rev. **112**, 815 (1961).

[7] J. Singh, *Excitation Energy Transfer Processes in Condensed Matter* (Plenum, N.Y., 1994).

[8] J.E. Jaffe, Nucl. Instr. and Methods in Phys. Res. A**580**, 1378 (2007); D.J. Robbins, J. Electrochem. Soc.: Solid-State Sci. Tech. **127**, 2694 (1980).

[9] C. Klingshirn, Phys. Status Solidi (b) **71**, 547 (1975).

[10] G. Bizarri, W.W. Moses, J. Singh, A.N. Vasil'ev and R.T. Williams, Phys. Status. Solidi (c) (2008) in press.

[11] W. Mengesha, T. Taulbee, B. Rooney and J. Valentine, IEEE Trans Nucl. Sci. **45**, 456 (1998).

[12] M. Inokuti, Rev. Mod. Phys. **43** (1971) 297.

[13] R. Mayol and F. Salvat, J. Phys. B: At. Mol. Opt. Phys. **23** (1990) 2117.

[14] J. C. Ashley, J. Electron Spectrosc. Relat. Phenom. **28** (1982) 177.

[15] J. C. Ashley, J. Electron Spectrosc. Relat. Phenom. **46** (1988) 199.

[16] D. R. Penn, Phys. Rev. B **35** (1987) 482.

[17] H. Bethe, Ann. Physik. **5**, 325 (1930).

[18] G.F. Knoll, *Radiation Detection and Measurement*, 3rd Ed. (John Wiley and Sons, New York, N.Y., 2005) p. 31.

[19] S. C. Blankespoor, S. E. Derenzo, W. W. Moses, and C. S. Rossington, IEEE Trans. Nucl. Sci. NS-41, 698 (1994)

[20] H.B. Dietrich, A.E. Purdy, R.B. Murray and R.T. Williams, Phys.Rev. B**12**, 5894 (1973).

[21] G. Bourdon, I. Robert, I. Sagnes, and I. Abram, J. Appl. Phys. **92**, 6595 (2002).

[22] G. Garcia-Belmonte, J. M. Montero, E. M. Barea and J. Bisquert, J. Appl. Phys. **101,** 114506 (2007

[23] A. Haug, J. Phys. C. Solid State Phys. **16**, 4159 (1983).

[24]W.L. Emkey, A.B.Romberger, and W.J. Van Sciver, Phys.Rev. B**20**, 5326(1979).

[25] http://physics.nist.gov/PhysRefData/Star/Text/ESTAR-u.html

[26] P. Dorenbos, R. Visser, C. W. E. van Eijk, J. Valbis, and N. M. Khaidukov, IEEE Trans. Nucl. Sci. **39**, 506 (1992).

[27] S. Shimizu, H. Ishibashi, A. Ejiri, and S. Kubota, Nucl. Inst. Meth. in Phys. Res. A **486**, 490 (2002).

[28] G. Bizarri and P. Dorembos, Phys. Rev. B**75**, 184302 (2007).

[29] A. N. Vasil'ev, IEEE Trans. Nucl. Sci. **55**, 1054 (2008).

[30] G. Bizarri, N. J. Cherepy, W.-S. Choong, G. Hull, W. W. Moses, S. A. Payne, J. Singh, J. D. Valentine, A. N. Vasil'ev, and R. T. Williams, IEEE Trans. Nucl. Sci., submitted for publication.

[31] e.g., S.M. Sze and K. K. Ng, *Physics of Semiconductor Devices*, 3rd Ed. (John Wiley & Sons, N.J., 2007).

[32] R. K. Ahrenkiel and F. C. Brown, Phys.Rev. A**136**, 223 (1964)].

[33]B. P. Aduev, E. D. Aluker, G. M. Belokurov, and V. N. Shvayko, phys. stat. sol. (b) **208**, 137 (1998)]

[34] R. T. Williams and A. K. Song, *Self-trapping of Excitons* (Springer, Berlin, 1993).

[35] P. A. Rodnyi, *Physical Processes in Inorganic Scintillators* (Boca Raton, CRC Publisher, 2007).

[36] http://hyperphysics.phy-astr.gsu.edu/hbase/electric/capcyl.html

[37] D. E. Cullen, J. H. Hubbell, and L. Kissel, EPDL97: the Evaluated Photon Data Library, '97 Version, Lawrence Livermore National Laboratory, UCRL--50400, Vol. 6, Rev. 5, September 1997.

[38] D. I. Vaisburd and K. E. Evdokimov, phys. stat. sol. (c) **2** (2005) 216.

[39] M.A.Terekhin, A.N.Vasil'ev, M.Kamada, E. Nakamura, S.Kubota, Phys. Rev. **B52** (1995) 3117.

[40] Glukhov R.A., Kamada M., Kubota S., Nakamura E., Ohara S., Terekhin M. A., Vasil'ev A. N., Proc. Int. Conf. on Inorganic Scintillators and Their Applications, SCINT95, Delft University Press, The Netherlands, 1996, p. 204.

Table I. Rate constants and other parameters used to calculate the scintillation light yield versus particle energy curves for four materials. Values in bold type were determined from independent measurements and considerations as discussed. Values in normal type were constrained as constants common to all four materials since they could only be roughly estimated. Values in italics are varied as fitting parameters among the four materials. References and estimations used in deducing or declaring these parameters are given in the text discussion.

Rate Constants	NaI:Tl	BaF_2	GSO:Ce	$LaCl_3$:Ce
R_{1x}	**4.7 x 10^6 s^{-1}**	**1.6 x10^9 s^{-1}**	**3 x10^7 s^{-1}**	**3 x10^7 s^{-1}**
K_{1x}	**1.2 x 10^6 s^{-1}**	**4 x10^8 s^{-1}**	**3 x10^6 s^{-1}**	**3 x10^6 s^{-1}**
R_{1eh}	**0**	**0**	**0**	**0**
K_{1eh}	3 x10^6 s^{-1}	3 x10^6 s^{-1}	3 x10^6 s^{-1}	3 x10^6 s^{-1}
R_{2eh}	**3 x 10^{-11} cm^3/s**	3x10^{-11} cm^3/s	3x10^{-11} cm^3/s	3x10^{-11} cm^3/s
K_{2eh}	3 x 10^{-12} cm^3/s	3 x 10^{-12} cm^3/s	3 x 10^{-12} cm^3/s	3 x 10^{-12} cm^3/s
R_{2x}	**0**	**0**	**0**	**0**
K_{2x}	2 x 10^{-11} cm^3/s	2 x 10^{-11} cm^3/s	2 x 10^{-11} cm^3/s	2 x 10^{-11} cm^3/s
K_{3eh}	1 x 10^{-29} cm^6/s	1 x 10^{-29} cm^6/s	1 x 10^{-29} cm^6/s	1 x 10^{-29} cm^6/s
K_{3x}	1 x 10^{-29} cm^6/s	1 x 10^{-29} cm^6/s	1 x 10^{-29} cm^6/s	1 x 10^{-29} cm^6/s
$\gamma_{eh\text{-}x}$	0	0	0	0
$\gamma_{x\text{-}eh}$	0	0	0	0
f_x (ex fraction)	*0.1*	*1*	*1*	*0.6*
r (track rad.)	*6 nm*	*2 nm*	*4 nm*	*4 nm*

Figure Captions

Fig. 1: The relative light output (total light yield) versus incident energy measured by Mengesha et al. [11]. (a) for seven materials, CaF_2:Eu, LSO, YAP, BGO, GSO, BaF_2, $LaCl_3$:Ce which show no hump in the yield and (b) for three materials, NaI:Tl, CsI:Tl and CsI:Na which show a hump in the yield.

Fig. 2(a) The local light yield (Y_L) plotted as a function of (-*dE/dx*) (keV/cm) from Eq. (8) for: NaI:Tl (1), BaF_2: Ce (2), GSO:Ce (3) and $LaCl_3$:Ce (4). Rates used for different materials are given in Table I.

Fig. 3: The total light yield (Y) plotted as a function of the total energy(E) (keV) from Eq. (11) for NaI:Tl (1), BaF_2: Ce (2), GSO:Ce (3) and $LaCl_3$:Ce (4). Rates used for different materials are given in Table I.

Fig. 4 : (a) The local light yield plotted as a function of (-dE/dx) calculated using Eq.(8) and (b) total light yield as a function of the total energy calculated using Eq. (11) for NaI:Tl scintillating crystals with f_x = 0.1, average track radius 6 nm and using rates from Table I. The dotted line curve corresponds to γ_{ex}=10^7 s^{-1} (γ_{xe}=9.86x10^5 s^{-1}) and solid line corresponds to γ_{ex}=10^5 s^{-1} (γ_{xe}=9.86x10^3 s^{-1}).

Fig. 5. Energy loss function $\mathrm{Im}\left(-\varepsilon^{-1}(\omega, q)\right)$ multiplied by the energy loss $\hbar\omega$ versus energy loss $\hbar\omega$ for different values of q ($E_q = \hbar^2 q^2 \ 2m$).Upper panel is for E $\leq$ 1keV and lower panel is for E $\geq$ 1keV.

Fig. 6. Top panel: Electron stopping power $-dE\,dx$ (left y-axis) for NaI crystal (E_g=5.9 eV, specific gravity = 3.7 g/cm^3); right axis shows the corresponding density of excitations at the track axis for mean themalization length r_{th} = 3 nm. Bottom panel: Mean free path for electron-electron scattering for NaI (black curve) and mean energy loss per a scattering (gray curve).

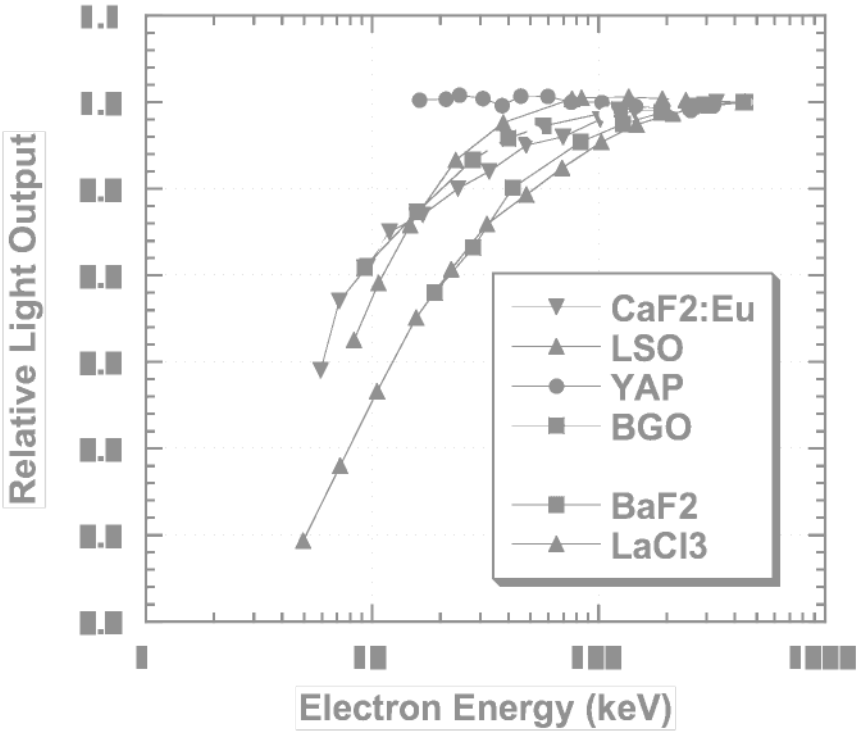

Fig. 1 (a): Bizarri et al. JAP

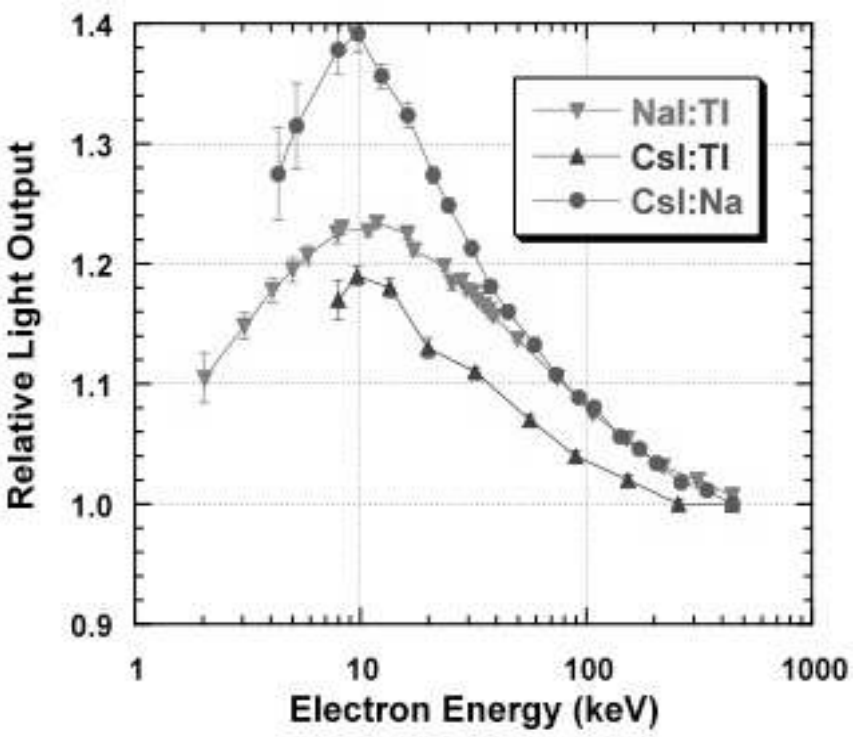

Fig. 1 (b): Bizarri et al., JAP

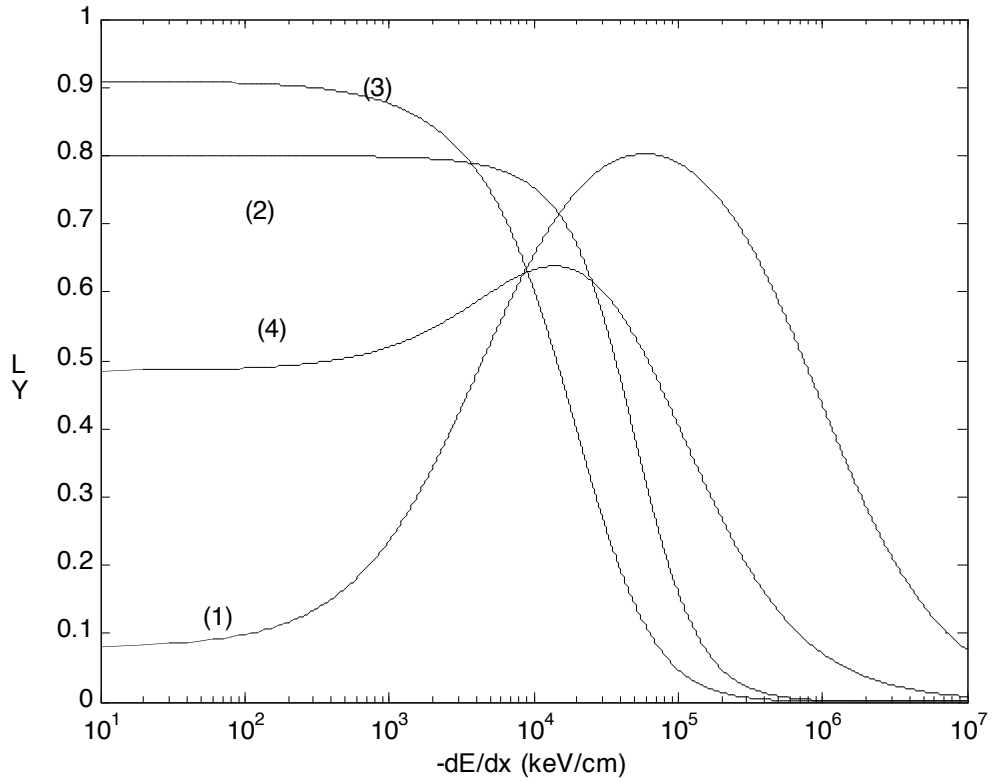

Fig.2 : Bizarri et al., JAP

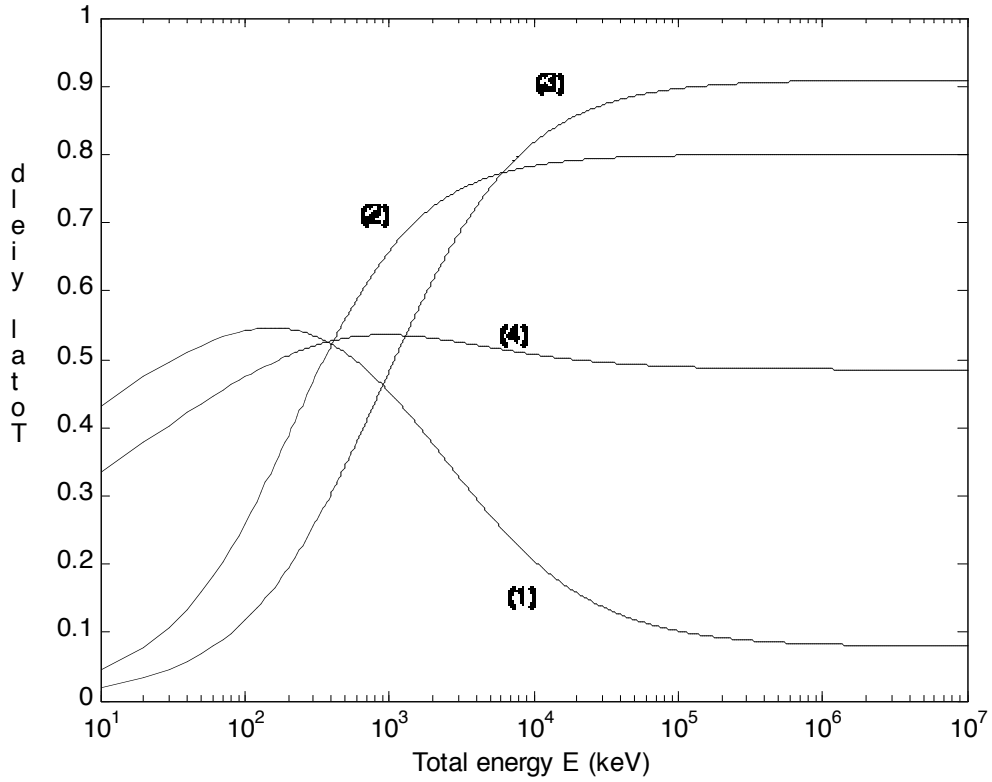

Fig.3 : Bizarri et al., JAP

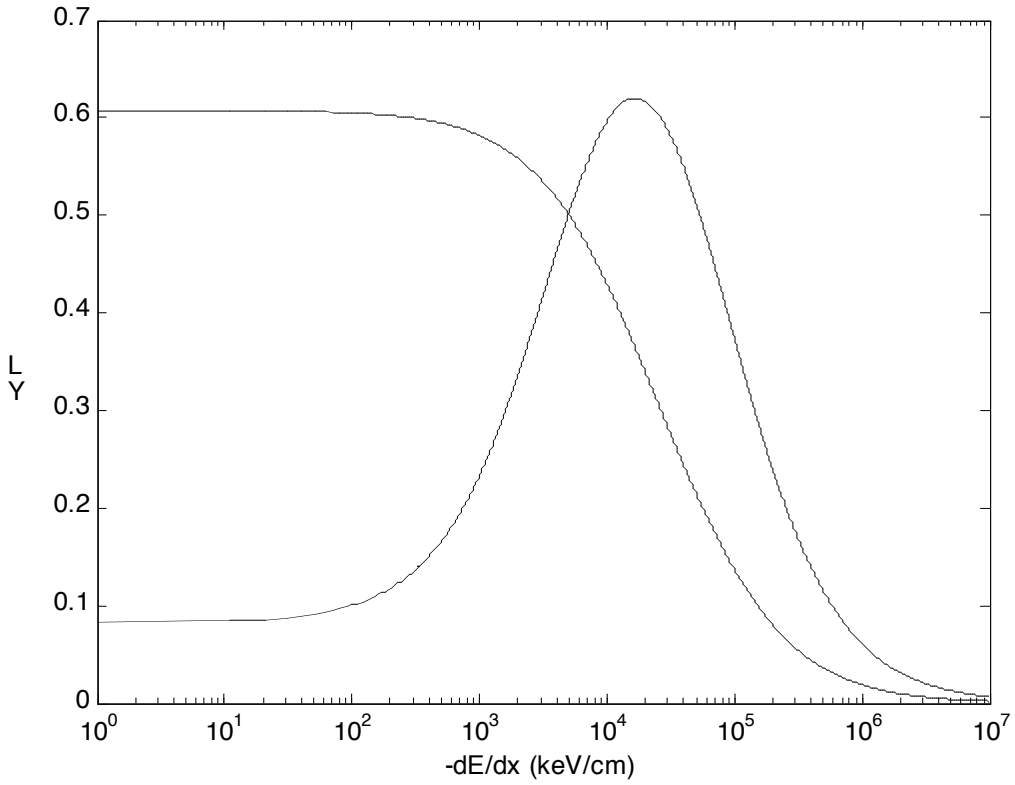

Fig.4 (a) : Bizarri et al., JAP

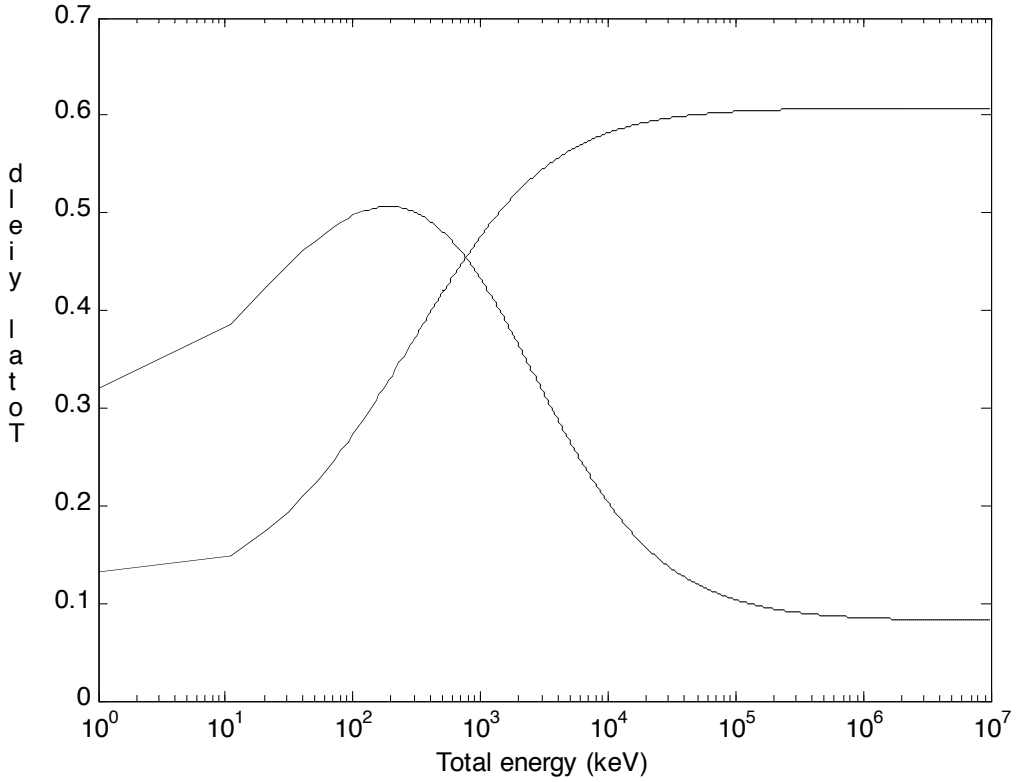

Fig.4(b) : Bizarri et al., JAP

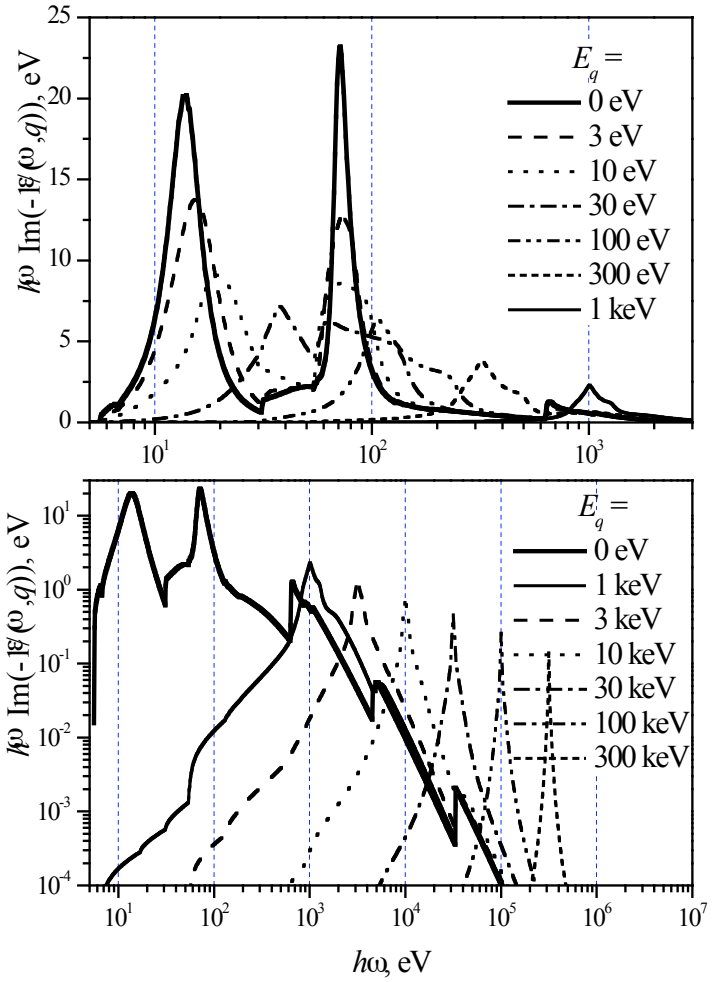

Fig.5 : Bizarri et al., JAP

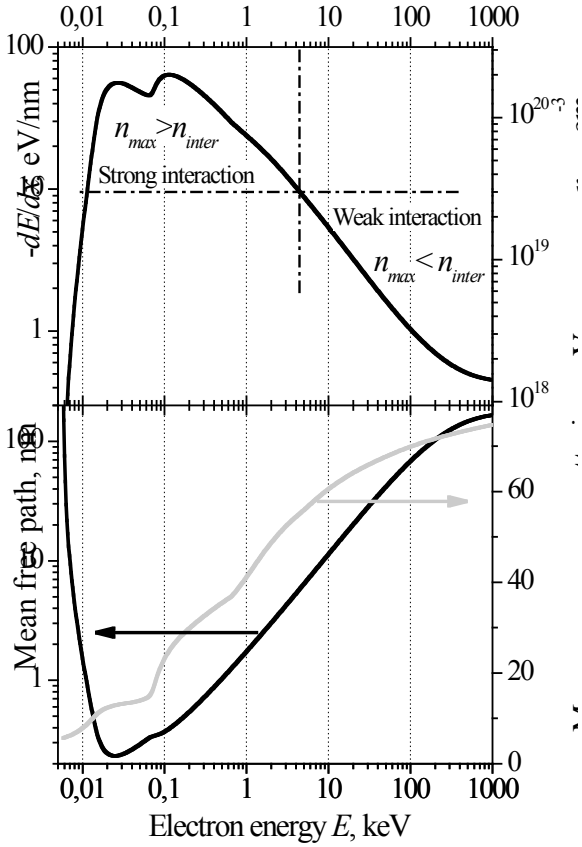

Fig.6 : Bizarri et al., JAP